Supporting Information

Peng et al. 10.1073/pnas.1311827110

SI Text

Methods and Models

First, we briefly describe the dissipative particle dynamics (DPD) method. Second, we present details of the two-component red blood cell (RBC) model, including the elasticity of both the lipid bilayer and the cytoskeleton, the bilayer–cytoskeletal interactions, and membrane viscosities. Third, we derive the scaling relationships between model units and physical units.

Dissipative Particle Dynamics. The DPD method is a particle-based mesoscopic simulation technique that allows modeling of fluids and soft matter. A DPD system is represented by N particles, which interact through pairwise effective potentials and move according to Newton's second law (1, 2). In a DPD simulation, a particle represents the center of mass in a cluster of atoms, and the position and momentum of the particle are updated in a continuous phase but spaced at discrete time steps. Particles i and j at positions r_i and r_j interact with each other via pairwise conservative, dissipative, and random forces, which are given by

$$F_{ij}^{C} = a_{ij}\omega(r_{ij})\mathbf{n}_{ij}, \qquad [S1]$$

$$F_{ij}^{D} = -\gamma\omega^2(r_{ij})(\mathbf{n}_{ij}\cdot\mathbf{v}_{ij})\mathbf{n}_{ij}, \qquad [S2]$$

$$F_{ij}^{R} = \sigma\omega(r_{ij})\zeta_{ij}\Delta t^{-1/2}\mathbf{n}_{ij}, \qquad [S3]$$

where $\mathbf{r}_{ij} = \mathbf{r}_i - \mathbf{r}_j$, $r_{ij} = |\mathbf{r}_{ij}|$, $\mathbf{n}_{ij} = \mathbf{r}_{ij}/r_{ij}$, and $\mathbf{v}_{ij} = \mathbf{v}_i - \mathbf{v}_j$. The coefficients a_{ij}, γ, and σ define, respectively, the strength of conservative, dissipative, and random forces. In addition, ζ_{ij} is a random number with zero mean and unit variance, and Δt is the time-step size. The weight function $\omega(r_{ij})$ is given by

$$\omega(r_{ij}) = \begin{cases} 1 - r_{ij}/r_c & r_{ij} < r_c \\ 0 & r_{ij} \geq r_c, \end{cases} \qquad [S4]$$

where r_c is the cutoff radius, which gives the extent of the interaction range. In the DPD method, the dissipative force and the random force act as heat sink and source, respectively, and the combined effect of the two forces acts a thermostat. Also, a common choice of the soft repulsion for the conservative force permits us to use larger integration time steps than are usually allowed by the molecular dynamics (MD) simulation technique; thus, DPD is a simple but efficient simulation method that correctly represents hydrodynamic interactions.

Membrane Elasticity of the Two-Component RBC Model. In this unique two-component RBC model, the membrane is modeled by two different components, i.e., the lipid bilayer and the cytoskeleton, as shown in Fig. S1*A*. Specifically, each component is constructed by a 2D triangulated network with N_v vertices, where each vertex is represented by a DPD particle. Different from the one-component DPD model, the lipid bilayer has no shear stiffness but only bending stiffness and a very large local area stiffness, whereas the inner layer (cytoskeleton) has no bending stiffness but a large shear stiffness. The potential of the RBC membrane including these two different components is written as

$$U = U_s + U_b + U_{a+v} + U_{int}, \qquad [S5]$$

where U_s is the spring's potential energy from the cytoskeleton, given by

$$U_s = \sum_{j\in 1\ldots N_s}\left[\frac{k_B T l_m\left(3x_j^2 - 2x_j^3\right)}{4p(1-x_j)} + \frac{k_p}{(n-1)l_j^{n-1}}\right], \qquad [S6]$$

where N_s is the number of springs, l_j is the length of the spring j, l_m is the contour length, $x_j = l_j/l_m$, p is the persistence length, k_B is the Boltzmann constant, T is the temperature, k_p is the spring constant, and n is a parameter. The first term is a worm-like chain (WLC) model (3) and the second term is a repulsive force term. Note that in the finite-element simulation (4), instead of using this exponential form of repulsive force, a simple functional form C/A is used, where C is a constant and A is the area of the corresponding triangle in the spectrin network. To be consistent in the comparison with the finite-element method (FEM) simulation result, we also used the same function form C/A in the prestressed DPD simulation case of micropipette aspiration. The isotropic mean stress for an equilateral triangle in the network is given as

$$\overline{T} = -\frac{3lf_{\mathrm{WLC}}(l)}{4A} - \frac{C}{A^2}, \qquad [S7]$$

where l is the length of the spectrin link, $f_{\mathrm{WLC}}(l)$ is the force of the WLC model, and $A = \sqrt{3}l^2/4$.

In our simulations, we have $\overline{T} = 0$ for the lipid bilayer. For the cytoskeleton, we also have $\overline{T} = 0$ in the case of stress-free initial configuration, but in the case of prestressed initial configuration, $\overline{T}$ can be nonzero; e.g., $\overline{T} = -30$ pN/μm.

Also, U_b is the bending energy from the lipid bilayer, given by

$$U_b = \sum_{j\in 1\ldots N_s} k_b\left[1 - \cos(\theta_j - \theta_0)\right], \qquad [S8]$$

where k_b is the bending coefficient and $k_b = 2k_c/\sqrt{3}$, where k_c is the bending stiffness of the bilayer. Also, θ_j is the instantaneous angle between two adjacent triangles as shown in Fig. S1*B*, and θ_0 is the spontaneous angle, which is set to zero in our simulations. Finally, U_{a+v} corresponds to the area and volume conservation constraints from the lipid bilayer, given by

$$U_{a+v} = \sum_{j\in 1\ldots N_t}\frac{k_l(A_j - A_0)^2}{2A_0} + \frac{k_v\left(V^{tot} - V_0^{tot}\right)^2}{2V_0^{tot}}, \qquad [S9]$$

where N_t is the number of triangles in the lipid bilayer, A_j is the instantaneous triangle area as shown in Fig. S1*B*, and A_0 is the initial triangle area. V^{tot} is the current total RBC volume, and V_0^{tot} is the initial total RBC volume. Also, k_l and k_v are the bilayer local area constraint coefficient and the global volume constraint coefficient, respectively.

Bilayer–Cytoskeletal Interactions. In addition to the commonly used elastic potentials for the membrane, we invoke another term U_{int} to capture the interaction between the lipid bilayer and the cytoskeleton, which can be expressed as a summation of harmonic potentials given by

$$U_{int} = \sum_{j\in 1\ldots N_{bs}}\frac{k_{bs}(d_j - d_{j0})^2}{2}. \qquad [S10]$$

Here N_{bs} is the number of bond connections between the bilayer and the cytoskeleton, i.e., the interactions between the transmembrane proteins (band 3 and glycophorin C) and spectrins, which is set to be the same as the number of vertices N_v in the current model; k_{bs} denotes the spring constant of the bond. Although there are two kinds of interactions in each junctional complex, including the major connections via band 3 and ankyrin and the secondary connections via actin, glycophorin C, and band 4.1, here we consider them together as an effective bilayer–cytoskeletal interaction in one junctional complex and model this interaction as a normal viscoelastic spring along with a tangential friction force as shown in Fig. S1 *C* and *D*. As shown in Fig. S1*C*, d_j is the distance between the vertex j of the cytoskeleton and the corresponding projection point j' on the lipid bilayer; and d_{j0} is the initial distance between the vertex j and the point j', which is set to zero in our simulations. Experiments show that $d_{j0} \approx 30$ nm (5), but we found that the difference is negligible in our simulations. Also, $\mathbf{n}_j$ is the normal direction of the lipid-bilayer surface at the projection point of vertex j. Numerically, a master–slave penalty contact algorithm is applied to calculate the force (6). The vertex in the spectrin cytoskeletal network is projected onto the closest triangle face of the lipid bilayer, and the distance and relative velocity between the cytoskeleton vertex and its projection point on the lipid bilayer are obtained as shown in Fig. S1*C*.

The corresponding elastic force on the vertex j of the cytoskeleton is given as

$$\mathbf{f}_j^E = k_{bs}(d_j - d_{j0})\mathbf{n}_j, \qquad \text{[S11]}$$

and the vertical damping force related to this elastic spring is

$$\mathbf{f}_j^D = -c_{bs}(\mathbf{v}_j \cdot \mathbf{n}_j)\mathbf{n}_j, \qquad \text{[S12]}$$

where c_{bs} is the vertical damping coefficient, and $\mathbf{v}_j$ is the relative velocity between the vertex j and the corresponding projection point j' on the lipid bilayer. The tangential friction force between the lipid bilayer and the cytoskeleton is given as

$$\mathbf{f}_j^F = -f_{bs}\left[\mathbf{v}_j - (\mathbf{v}_j \cdot \mathbf{n}_j)\mathbf{n}_j\right], \qquad \text{[S13]}$$

where f_{bs} is the tangential friction coefficient.

To ensure that the temperature is constant, another random force term is added, as in ref. 7,

$$\mathbf{f}_j^R \Delta t = \sqrt{2k_{\mathrm{B}}T}\left(\sqrt{2f_{bs}}d\mathbf{W}_{ij}^A + \sqrt{3c_{bs}}\,\frac{tr[d\mathbf{W}_{ij}]}{3}1\right)\cdot\mathbf{n}_j, \qquad \text{[S14]}$$

where $tr[d\mathbf{W}_{ij}]$ is the trace of a random matrix of independent Wiener increments of $d\mathbf{W}_{ij}$. The Wiener increment $d\mathbf{W}_{ij}(t) = \mathbf{W}_{ij}(t+\Delta t) - \mathbf{W}_{ij}(t)$ over a time-step Δt is a random variable drawn from a normal distribution with zero mean and a time-step variance $\mathcal{N}[0, \Delta t]$. $d\mathbf{W}_{ij}^A = (d\mathbf{W}_{ij} - d\mathbf{W}_{ji})/2$ is the antisymmetric part, and Δt is the magnitude of the time step.

Hence, the total interaction force is given by

$$\mathbf{f}_j^{int} = \mathbf{f}_j^E + \mathbf{f}_j^D + \mathbf{f}_j^F + \mathbf{f}_j^R. \qquad \text{[S15]}$$

In addition, $\mathbf{f}_j^{int}$ is also distributed to the three vertices of the corresponding bilayer triangle with one-third of the magnitude and an opposite sign to follow Newton's third law. For simplicity, the vertical damping coefficient is always set to be the same as the friction coefficient; i.e., $c_{bs} = f_{bs}$.

Membrane Viscosities. The membrane viscosity is incorporated into both the lipid bilayer and the cytoskeleton by adding two terms, i.e., dissipative and random forces, respectively, as

$$\mathbf{F}_{ij}^{D,k} = -\gamma_k^T \mathbf{v}_{ij} - \gamma_k^C(\mathbf{v}_{ij}\cdot\mathbf{e}_{ij})\mathbf{e}_{ij}, \qquad \text{[S16]}$$

$$\mathbf{F}_{ij}^{R,k}\Delta t = \sqrt{2k_{\mathrm{B}}T}\left(\sqrt{2\gamma_k^T}d\overline{\mathbf{W}}_{ij}^S + \sqrt{3\gamma_k^C - \gamma_k^T}\,\frac{tr[d\mathbf{W}_{ij}]}{3}1\right)\cdot\mathbf{e}_{ij}, \qquad \text{[S17]}$$

where γ_k^T and γ_k^C are dissipative parameters ($3\gamma_k^C > \gamma_k^T$); and $\mathbf{e}_{ij}$ and $\mathbf{v}_{ij}$ are the relative position and velocity vectors of spring ends i and j. Also, $d\overline{\mathbf{W}}_{ij}^S = d\mathbf{W}_{ij}^S - tr[d\mathbf{W}_{ij}^S]1/3$ is the traceless symmetric part of the random matrix of independent Wiener increments of $d\mathbf{W}_{ij}$, and $k = b, s$ stands for the lipid bilayer or the cytoskeleton, respectively. The viscosities of the lipid bilayer and the cytoskeleton can be calculated as

$$\eta_k = \sqrt{3}\gamma_k^T + \frac{\sqrt{3}\gamma_k^C}{4}. \qquad \text{[S18]}$$

Experiments show that the cytoskeleton viscosity η_s is about 50–100 times larger than the lipid-bilayer viscosity η_b (8).

Scaling of DPD Model and Physical Units. Within the DPD approach, reduced units are used for the mass, length, and energy. In the following, we derive the scaling relationships between model units and physical units.

Let $r = 1$ m denote the length scale in the physical system in SI units and r' denote the length scale of the DPD model. The same initial diameter ($D_0 = 7.82$ μm) of the RBC can be expressed in both the DPD system and the physical system as

$$D_0 = D_0^M \cdot r' = D_0^P \cdot r = 7.82 \times 10^{-6}\ \mathrm{m}, \qquad \text{[S19]}$$

where $D_0^P = 7.82 \times 10^{-6}$ and m is meter. The variables with upper index "P" (e.g., D_0^P) are values (numbers without units) of the quantities (e.g., D_0) in the physical system with SI units, whereas the variables with upper index "M" (e.g., D_0^M) are values (numbers without units) of the quantities (e.g., D_0) in the DPD system. We can choose the length-scale r' of the DPD system, and usually specific values of r' and D_0^M depend on the size of the DPD system.

Because

$$\left[\frac{k_{\mathrm{B}}T}{\mu_s}\right] = \mathrm{length}^2, \qquad \text{[S20]}$$

where $[\cdot]$ denotes the dimension of a quantity, μ_s is the shear modulus, k_{B} is the Boltzmann constant, and T is the temperature, we should have

$$\frac{k_{\mathrm{B}}T}{\mu_s} = \frac{(k_{\mathrm{B}}T)^M}{\mu_s^M}(r')^2 = \frac{(k_{\mathrm{B}}T)^P}{\mu_s^P}(r)^2. \qquad \text{[S21]}$$

Plugging Eq. **S19** into Eq. **S21**, we get

$$(k_{\mathrm{B}}T)^M = \frac{\mu_s^M}{\mu_s^P}\left(\frac{D_0^M}{D_0^P}\right)^2 (k_{\mathrm{B}}T)^P. \qquad \text{[S22]}$$

Similarly for the force N, because

$$\left[\frac{k_{\mathrm{B}}T}{N}\right] = \mathrm{length}, \qquad \text{[S23]}$$

we have

$$N^M = \frac{(k_{\mathrm{B}}T)^M}{(k_{\mathrm{B}}T)^P}\frac{r^M}{r^P}N^P = \frac{(k_{\mathrm{B}}T)^M}{(k_{\mathrm{B}}T)^P}\frac{D_0^P}{D_0^M}N^P = \frac{\mu_s^M}{\mu_s^P}\frac{D_0^M}{D_0^P}N^P. \qquad \text{[S24]}$$

For time scaling, because

$$\left[\frac{\eta D_0^2}{N}\right] = \text{time}, \qquad \textbf{[S25]}$$

where η is a characteristic viscosity, we have

$$\frac{\eta D_0^2}{N} = \frac{\eta^M \left(D_0^M\right)^2}{N^M}\tau' = \frac{\eta^P \left(D_0^P\right)^2}{N^P}\tau, \qquad \textbf{[S26]}$$

where $\tau = 1$ s is the timescale in the physical system with SI units, and τ' is the timescale in the DPD system. Plugging Eq. **S24** into Eq. **S26**, we get the timescale of the DPD system as

$$\tau' = \frac{D_0^P}{D_0^M}\frac{\eta^P}{\eta^M}\frac{\mu_s^M}{\mu_s^P}\ \text{s}, \qquad \textbf{[S27]}$$

where s denotes second.

For example, in the simulations of tank-treading motions, the RBC diameter, the membrane Young's modulus, and the interior fluid viscosity are $D_0^M = 7.82$, $\mu_s^M = 12.125$, and $\eta^M = 1.8$, respectively, corresponding to $D_0^P = 7.82 \times 10^{-6}$, $\mu_s^P = 4.725 \times 10^{-6}$, and $\eta^P = 0.006$ in the physical system with SI units. Hence, the DPD timescale is $\tau' \simeq 2.7$ ms. In the simulations of tank-treading motions, a time-step size $\Delta t^M = (0.0005 \sim 0.005)$ in DPD units is used, which gives $\Delta t = \Delta t^M \tau' = (1.35 \sim 13.5)$ μs.

Comparison with Existing Models. Two-component whole-cell erythrocyte membrane models have been developed before (4, 9, 10). Compared with the existing models, the current two-component DPD model has three major advantages. The first advantage is that we explicitly model the bilayer–cytoskeletal interaction including the normal interaction and tangential friction based on realistic protein connectivity, in such a way that the bilayer–cytoskeletal interaction force and cytoskeleton deformation at the molecular level can be investigated directly. Second, we use a systematic coarse-graining procedure starting from the spectrin level (11, 12) so that different coarse-graining levels can be used to produce adequate levels of desired accuracy. Third, the model proposed here can predict the physical phenomena of quasi-static deformation, fluid dynamics, and thermal fluctuations, whereas some of the prior two-component whole-cell models (4, 10) cannot simulate thermal fluctuations. In addition, in contrast to the existing particle-based two-component model (9), our thermal fluctuation simulations have been validated extensively by comparing the results with experimental data (13).

In addition to two-component whole-cell models, there are also sophisticated two-component models of local membranes, in which only a small piece of RBC membrane is simulated, such as the model by Li and Lykotrafitis (14). Their model is more detailed with molecular information on lipid diffusion. Consequently, the computational cost is prohibitively high for it to be applicable to study whole-cell problems at the present time. However, the computational framework we present here can be further extended in future work to include these extra details as studied in ref. 14. As the first step, and for computational expediency, we neglect these details here and focus on the problems of the whole cell, such as in rheology, where details like lipid diffusion are not important. Hence, our two-component model is a good compromise between the one-component whole-cell DPD model and the two-component detailed molecular dynamics model in ref. 14. It can be used to explore important problems involving cell physiology and pathological states mediated by protein mutations, such as the bilayer loss in hereditary spherocytosis and the bilayer–cytoskeleton uncoupling in sickle-cell anemia (15).

Simulation Setups and Parameter Estimation

Here, we present details of the simulation setups of micropipette aspiration, membrane fluctuations, tank-treading motion, and channel flow stretching. Subsequently, we estimate the default main parameters.

Micropipette Aspiration Simulation Setup. In the micropipette aspiration (16), a negative pressure is applied to aspirate a RBC into a small glass pipette. The RBC membrane undergoes large deformation during this aspiration process. To measure the area deformation of the cytoskeleton alone, the actins in the RBC membrane are labeled using rhodamine–phalloidin, an antibody with fluorescence. By measuring the fluorescence light intensity, the actin density in different regions of the cytoskeleton can be determined, which is inversely proportional to the area deformation of the cytoskeleton. It was found that the cytoskeleton in the cap region of the aspirated cell inside the pipette is significantly expanded, whereas the cytoskeleton near the pipette entrance is compressed. The density of the lipid molecule marked by another antibody was found uniform over the cell surface because the lipid bilayer is incompressible. This experiment takes up to 30 min to allow the bilayer–cytoskeletal slip to reach steady state, so that it is modeled as a quasi-static process in our simulation; i.e., the bilayer–cytoskeletal friction and membrane viscosities are neglected. The parameters used in this simulation are listed in Table S1.

The RBCs are hypotonically swollen (osmotic pressure is in a typical range of 160–250 mOsm) in the beginning of this experiment (16) and correspondingly our RBC model is also inflated from a standard biconcave shape accordingly in the beginning of the simulation. A rigid cylindrical surface is used to represent the pipette. The interaction between the lipid bilayer and the pipette is modeled as a hard contact by using a master–slave algorithm (6) similar to the bilayer–cytoskeletal interaction but with a large spring constant. As indicated in the experiments, during the aspiration the membrane is usually separated from the pipette by a small gap of fluid so that the friction between them is insignificant and thus not considered in our model. We further simplify the fluid pressure distribution inside the pipette as a uniform pressure difference applied on the cap region of the lipid bilayer and a linear distribution along the aspiration length; the pressure difference equals zero at the entrance.

In addition to the results shown in Fig. 1 in the main text, we also applied the one-component DPD model to study this problem, and we found that the area expansion is abnormally large in the cap region. The reason is that we applied a uniform pressure on the cap region of the cell with a linear distribution along the aspiration length, which is different from the interaction pressure applied on the cytoskeleton from the lipid bilayer in the two-component model. Basically, the large local area modulus of the bilayer is absent in the one-component DPD model. In the Monte Carlo simulation (3), instead of applying the pressure to deform the cell, a canonical shape (cylinder/sphere) was assumed; the vertices of the triangular network were allowed to slide along this assumed shape.

Membrane Fluctuations Simulation Setup. We use the two-component DPD model to simulate membrane fluctuations. Because cells adhere to the substrate in the experiment, we fixed 13% of vertices on the RBC bottom and the simulations show that the effect of attachment strength (percentage of fixed vertices on the RBC bottom) on the amplitude fluctuations is negligible as long as more than 13% of the vertices are fixed (13). The extracellular and intracellular fluids with different viscosities were modeled using DPD particles. The top surface with a radius of 3 μm was monitored.

We did not use the full resolution model to study this problem because of computational cost. To reach the same timescale, the full resolution model with $N_v = 23{,}867$ is about 8,000 times more

expensive than the model with $N_v = 500$. The latter takes 1 h to run a typical case on a 32-core 800-MHz node.

Although we invoke a systematic coarse-graining approach (11, 12) for the in-plane mechanical properties such as shear modulus in the current study, the proper coarse-graining procedure for the properties of the bilayer–cytoskeletal interaction in the vertical direction in thermal fluctuations is unclear. For example, if we assume $k_{bs} = k_{bs}^{23,867}$ in the full resolution model with $N_v = 23{,}867$ and $k_{bs} = k_{bs}^{500}$ in the coarse-grained model with $N_v = 500$, it can be derived that $k_{bs}^{500} = 23{,}867/500 \cdot k_{bs}^{23,867} \approx 48 \cdot k_{bs}^{23,867}$, because $k_{bs}^{23,867}$ represents the stiffness of one junctional complex connection whereas k_{bs}^{500} represents the stiffness of 48 junctional complex connections. However, simulation results show this simple coarse-graining procedure makes the 500 DPD particle model too stiff in membrane fluctuation simulations. Lumping of 48 junctional complexes into one connection means that these junctional complexes always move with the same displacement, but in reality or in the simulation using the full resolution model with $N_v = 23{,}867$, the fluctuations of these 48 junctional complexes follow a distribution and their motions are not synchronized. Instead, simulations show that more reasonable results can be obtained by using $k_{bs}^{500} \approx k_{bs}^{23,867}$. Therefore, in the simulations of membrane fluctuations, we use the same physical values of k_{bs}, c_{bs}, and f_{bs} for different coarse-graining levels. For other simulations such as micropipette aspiration and tank-treading motion, we found the effect of k_{bs} is insignificant. The parameters used in this simulation are listed in Table S1.

Tank-Treading Simulation Setup. In the simulations of the tank-treading (TT) motion of a RBC in shear flow, we place a single RBC in linear shear flow between two planar solid walls and simulate the TT motion at different shear rates, using both the one-component and the two-component RBC models. The no-slip boundary condition between the fluid and the solid wall and that between the fluid and the RBC membrane are enforced using the bounce-back condition (17). The viscosity of the suspending medium is specified as $\eta_0 = 0.0289$ Pa s based on the experiment (18) and the viscosity of the cytosol inside the RBC is given as $\eta_1 = 0.006$ Pa s (19). For the membrane viscosities, it was found that the viscosity of the cytoskeleton is about 50 times larger than that of the lipid bilayer (8). By selecting the bilayer and cytoskeleton viscosities as $\eta_b = 0.008$ Pa s and $\eta_s = 0.372$ Pa s, respectively, the TT frequency matches the experimental results well as shown in Fig. 3*A* in the main text. Other parameters used in this simulation are listed in Table S1.

Channel Flow Stretching Simulation Setup. Channel flow stretching experiments have been carried out to examine the response of cells attached to a substrate to shear stresses exerted by an incoming flow. In a typical channel flow setup, erythrocytes are allowed to sediment inside a channel consisting of two parallel plates. The substrate is coated with BSA so that most cells do not adhere to the bottom plate with large attachment areas. When external flow is introduced, the cells deform while one point (in some cases more than one) remains attached to the substrate. Long membrane strands (tethers) may appear when the hydrodynamic shear exceeds a certain threshold value (~ 1.5 dyn/cm^2 or 0.15 pN/μm^2) (20).

In the simulation of whole-cell stretching with a line attachment between the cell and the substrate, two points at the bottom of the cell are fixed as shown in Fig. 4*A*, to create a line attachment. Because the line attachment edge of the cell was between 2 μm and 3 μm in the experiment, the distance between these two points is chosen with an average value of 2.5 μm in our simulations.

In the case with one attachment point, the cell attaches to the substrate not at a geometric point but within a small attachment area. In our model this attachment area is depicted as a circular area on the cell membrane whose diameter D_a is chosen to be 0.15 μm, which is within the same range as the diameter of the tether estimated from optical and scanning electron photomicrographs, i.e., 0.1–0.2 μm (20). It is important to note here that the two are not expected to be exactly the same, because the radius of the tether R_t depends on the applied force f_0 by the relation $R_t = 2\pi k_c / f_0$, where k_c is the bending stiffness (21).

Parameter Estimation. The default values of the main parameters of the two-component DPD model are listed in Table S1 for different cases. The initial membrane shear modulus without deformation μ_s is measured as 6 pN/μm in the micropipette aspiration experiment (19), but at a smaller value in the thermal fluctuations experiment (22). The shear modulus increases with deformation due to strain-induced stiffening (3) and may decrease at very large deformation due to spectrin unfolding (23). It can be one order higher for malaria-infected RBCs (24, 25). The bending modulus $k_c = 2.4 \times 10^{-19}$ J is a relatively well-accepted value (19). The membrane viscosity is measured as about 1.0 Pa s (26, 27), which is considered the sum of the bilayer viscosity η_b and the cytoskeleton viscosity η_s. According to Berk et al. (8), the cytoskeleton viscosity is 50–100 times larger than the bilayer viscosity. The membrane viscosity plays a significant role in tank-treading frequency (17) and by comparing predicted tank-treading frequency with experimental data we estimated typical values of η_b and η_s as shown in Table S1 and use them as default values.

The strength of the bilayer–cytoskeletal interaction bond is estimated on the order of 10 pN on a junctional complex in the current study by simulating the channel flow stretching experiment. If we assume the bond displacement to be around 0.2 μm when the bond breaks, a rough estimation of k_{bs} can be obtained as $k_{bs} = 10$ pN/0.2 μm = 50 pN/μm for a junctional complex. We used a default value of $k_{bs} = 46$ pN/μm as shown in Table S1. In addition, if we assume the stiffness of the bilayer–cytoskeletal interaction bond is in the same order of the stiffness of a spectrin, the linearized stiffness of a spectrin modeled using the WLC model is given as $k_{bs} = 3k_BT/2pL_c = 4$ pN/μm with a persistence length of $P = 7.5$ nm and contour length $L_c = 200$ nm (3); this can be considered as a lower-bound value. The bilayer–cytoskeletal friction coefficient f_{bs} has been estimated as 0.194 pN·μm^{-1}·s^{-1} for a single junctional complex based on the experimentally measured diffusivity of transmembrane proteins and the fluctuation dissipation theorem (10). For simplicity, the vertical damping coefficient is always set to be the same as the friction coefficient; i.e., $c_{bs} = f_{bs}$.

In addition to these main parameters, other parameters are given as follows: bilayer local area constraint $k_l = 5{,}000$ and global volume constraint $k_v = 5{,}000$ (both in DPD units). They serve as penalty parameters and their influence is negligible as long as their values are high enough. In Eq. **S7**, $n = 2$, $k_p = 1.0$, and $l_m = 2.2x_0$, where x_0 is the initial length of the spring in the cytoskeleton. The biconcave shape is chosen to be the stress-free state of the cytoskeleton, and $\theta_0 = 0$ in Eq. **S8**; i.e., the spontaneous curvature is zero.

One objective of the current study was to probe the mechanical characteristics associated with the bilayer–cytoskeletal viscoelastic interactions, which cannot be measured directly by existing experiments, and to investigate the effects of these mechanical parameters on overall experimental results. For example, in the fluorescence-marked micropipette aspiration experiments, we validate our model by predicting local cytoskeletal spectrin deformation. It mainly depends on the constitutive law of the cytoskeleton. Because it is a quasi-static process, the result is independent of dissipative parameters such as f_{bs}, η_b, and η_s; the influence of k_{bs} is found to be small as well. In the membrane fluctuations experiment, the amplitude of the fluctuations is independent of viscous parameters f_{bs}, η_b, and η_s (28, 29), and consequently we mainly study the effect of k_{bs} and μ_s. In the experiments involving tank-treading motion in shear flow, we focus on the effects of dissipative parameters f_{bs}, η_b, and η_s, because they play a major

role in influencing the tank-treading frequency. As for bilayer–cytoskeletal detachment in the channel flow experiments, our objective was to estimate bilayer–cytoskeletal bond strength σ_{bs}. Because only one or two parameters in each simulation of these four experiments are relevant to the result, our approach provides a good protocol in validating the two-component model and in investigating the effects of these parameters in isolation, in a systematic and controlled manner.

1. Hoogerbrugge PJ, Koelman JM (1992) Simulating microscopic hydrodynamic phenomena with dissipative particle dynamics. *Europhys Lett* 19(3):155–160.
2. Groot RD, Warren PB (1997) Dissipative particle dynamics: Bridging the gap between atomistic and mesoscopic simulation. *J Chem Phys* 107:4423–4435.
3. Discher DE, Boal DH, Boey SK (1998) Simulations of the erythrocyte cytoskeleton at large deformation. II. Micropipette aspiration. *Biophys J* 75(3):1584–1597.
4. Peng Z, Asaro RJ, Zhu Q (2010) Multiscale simulation of erythrocyte membranes. *Phys Rev E Stat Nonlin Soft Matter Phys* 81(3 Pt 1):031904.
5. Heinrich V, Ritchie K, Mohandas N, Evans E (2001) Elastic thickness compressibilty of the red cell membrane. *Biophys J* 81(3):1452–1463.
6. Malone JG, Johnson NL (1994) A parallel finite element contact/impact algorithm for nonlinear explicit transient analysis: Part I-The search algorithm and contact mechanics. *Int J Numer Methods Eng* 37:559–590.
7. Español P (1998) Fluid particle model. *Phys Rev E Stat Phys Plasmas Fluids Relat Interdiscip Topics* 57:2930–2948.
8. Berk DA, Hochmuth RM, Waugh RE (1989) Viscoelastic properties and rheology. *Red Blood Cell Membranes*, eds Agre P, Parker JC (Marcel Dekker, New York), pp 445–446.
9. Noguchi H, Gompper G (2005) Shape transitions of fluid vesicles and red blood cells in capillary flows. *Proc Natl Acad Sci USA* 102(40):14159–14164.
10. Peng Z, Asaro R, Zhu Q (2011) Multiscale modeling of erythrocytes in Stokes flow. *J Fluid Mech* 686:299–337.
11. Pivkin IV, Karniadakis GE (2008) Accurate coarse-grained modeling of red blood cells. *Phys Rev Lett* 101(11):118105.
12. Fedosov DA, Caswell B, Karniadakis GE (2010) Systematic coarse-graining of spectrin-level red blood cell models. *Comput Methods Appl Mech Eng* 199:1937–1948.
13. Fedosov DA, Lei H, Caswell B, Suresh S, Karniadakis GE (2011) Multiscale modeling of red blood cell mechanics and blood flow in malaria. *PLoS Comput Biol* 7(12):e1002270.
14. Li H, Lykotrafitis G (2012) Two-component coarse-grained molecular-dynamics model for the human erythrocyte membrane. *Biophys J* 102(1):75–84.
15. Liu SC, Derick LH, Zhai S, Palek J (1991) Uncoupling of the spectrin-based skeleton from the lipid bilayer in sickled red cells. *Science* 252(5005):574–576.
16. Discher DE, Mohandas N, Evans EA (1994) Molecular maps of red cell deformation: Hidden elasticity and in situ connectivity. *Science* 266(5187):1032–1035.
17. Fedosov DA, Caswell B, Karniadakis GE (2010) A multiscale red blood cell model with accurate mechanics, rheology, and dynamics. *Biophys J* 98(10):2215–2225.
18. Fischer TM (2007) Tank-tread frequency of the red cell membrane: Dependence on the viscosity of the suspending medium. *Biophys J* 93(7):2553–2561.
19. Mohandas N, Evans EA (1994) Mechanical properties of the red cell membrane in relation to molecular structure and genetic defects. *Annu Rev Biophys Biomol Struct* 23:787–818.
20. Hochmuth RM, Mohandas N, Blackshear PL, Jr. (1973) Measurement of the elastic modulus for red cell membrane using a fluid mechanical technique. *Biophys J* 13(8):747–762.
21. Waugh RE, Hochmuth RM (1987) Mechanical equilibrium of thick, hollow, liquid membrane cylinders. *Biophys J* 52(3):391–400.
22. Strey H, Peterson M, Sackmann E (1995) Measurement of erythrocyte membrane elasticity by flicker eigenmode decomposition. *Biophys J* 69(2):478–488.
23. Zhu Q, Asaro RJ (2008) Spectrin folding versus unfolding reactions and RBC membrane stiffness. *Biophys J* 94(7):2529–2545.
24. Suresh S, et al. (2005) Connections between single-cell biomechanics and human disease states: Gastrointestinal cancer and malaria. *Acta Biomater* 1(1):15–30.
25. Park Y, et al. (2008) Refractive index maps and membrane dynamics of human red blood cells parasitized by *Plasmodium falciparum*. *Proc Natl Acad Sci USA* 105(37): 13730–13735.
26. Abkarian M, Faivre M, Viallat A (2007) Swinging of red blood cells under shear flow. *Phys Rev Lett* 98(18):188302.
27. Tran-Son-Tay R, Sutera SP, Rao PR (1984) Determination of red blood cell membrane viscosity from rheoscopic observations of tank-treading motion. *Biophys J* 46(1): 65–72.
28. Milner ST, Safran SA (1987) Dynamical fluctuations of droplet microemulsions and vesicles. *Phys Rev A* 36(9):4371–4379.
29. Bivas I (2010) Shape fluctuations of nearly spherical lipid vesicles and emulsion droplets. *Phys Rev E Stat Nonlin Soft Matter Phys* 81(6 Pt 1):061911.

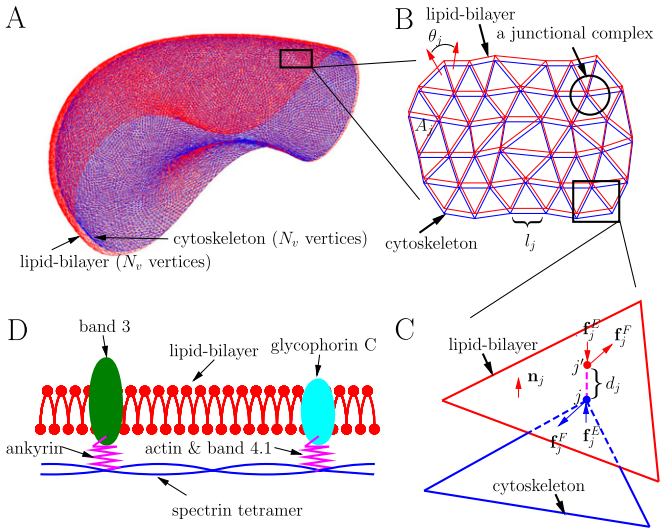

Fig. S1. (*A*) Two-component DPD model of the whole cell ($N_v = 23,867$, i.e., 23,867 DPD particles on each triangular network). (*B*) Local triangular networks of the two-component model: l_j is the spring length of the cytoskeleton; θ_j is the instantaneous angle between two adjacent triangles on the bilayer; and A_j is the triangle area. (*C*) Normal and tangential interactions between the lipid bilayer and the cytoskeleton. j' is the projection point on the lipid bilayer of vertex j on the cytoskeleton; d_j is the distance between point j and point j';$\mathbf{f}_j^F$ is the tangential friction interaction force, whereas $\mathbf{f}_j^E$ is the normal elastic interaction force; and $\mathbf{n}_j$ is the normal direction vector of the bilayer triangle. (*D*) Physical picture of the local bilayer–cytoskeletal interaction. Although there are two kinds of interactions in each junctional complex, including the major connections via band 3 and ankyrin and the secondary connections via actin, glycophorin C, and band 4.1, we consider them together as an effective bilayer–cytoskeletal interaction in one junctional complex and model it as a normal elastic force and a tangential friction force. The vertical damping force $\mathbf{f}_j^D$ and the random force $\mathbf{f}_j^R$ are not shown for clarity.

Table S1. Main parameters of the two-component DPD model

Study cases	μ_s, pN/μm	k_c, J	η_s, Pa s	η_b, Pa s	k_{bs}, pN/μm	f_{bs}, pN·μm^{-1}·s^{-1}
Default	6	2.4e-19	0.372	0.008	46.0	0.194
Micropipette	6	2.4e-19	Independent	Independent	46.0	Independent
Fluctuations	Table S2	2.4e-19	Independent	Independent	Fig. 2*A*	Independent
Tank treading	6	2.4e-19	0.372	0.008	46.0	Fig. 3*B*
Channel flow	6	2.4e-19	Independent	Independent	46.0	Independent

μ_s, initial cytoskeleton shear stiffness (19); k_c, bilayer bending stiffness (19); η_s, cytoskeleton viscosity (27); η_b, bilayer viscosity (8, 27); k_{bs} and f_{bs}, the elastic and friction coefficients of the bilayer–cytoskeletal interactions (10).

Table S2. Shear moduli of healthy RBCs and ring-stage RBCs at the physiological and febrile temperatures obtained in ref. 25

Healthy, 37 °C, pN/μm	Healthy, 41 °C, pN/μm	Ring, 37 °C, pN/μm	Ring, 41 °C, pN/μm
6.2	4.9	14.5	20.4